CHALMERS
UNIVERSITY OF TECHNOLOGY

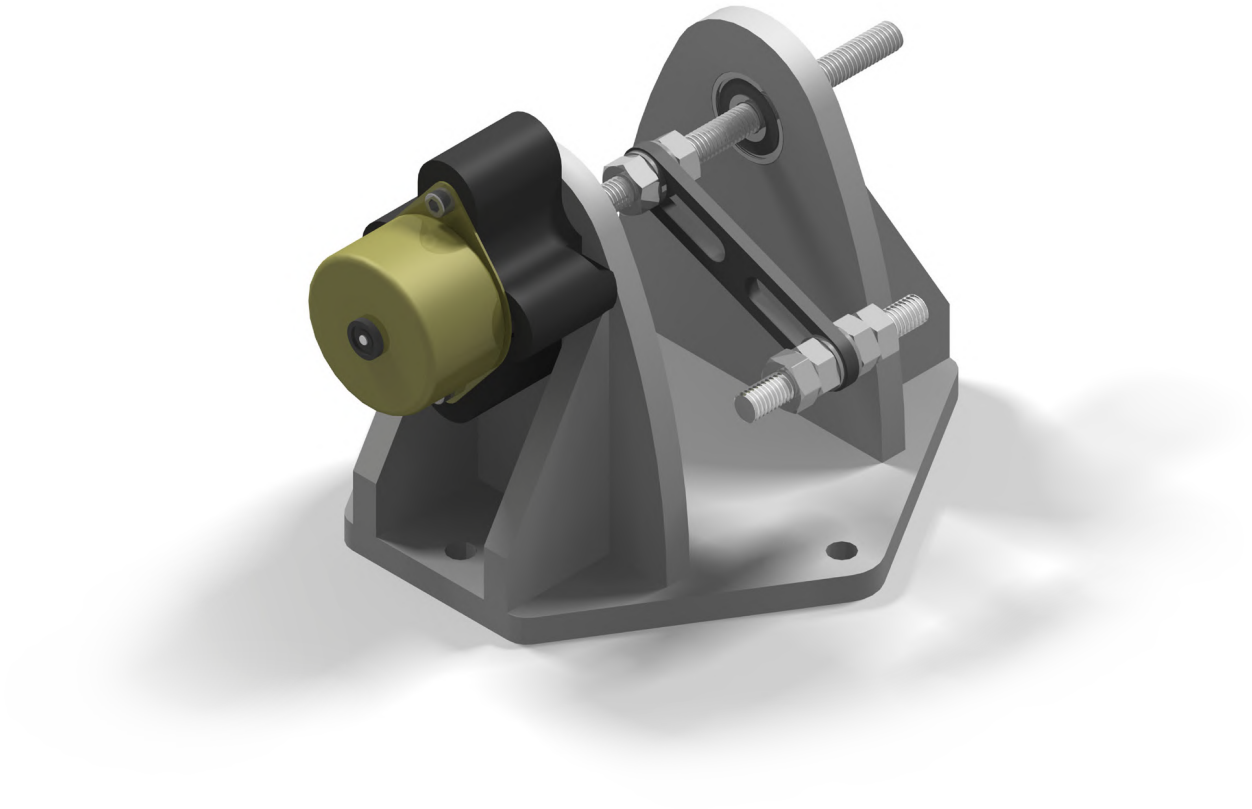

Rotational vibration energy harvester

Development of a system model to predict dynamic response of a rotational electromagnetic vibration energy harvester

Master's thesis in Electrical Engineering

MAX CHRISTENSEN
JONATHAN ULMESTRAND

CHALMERS UNIVERSITY OF TECHNOLOGY
Gothenburg, Sweden 2021

Master's thesis in Electrical Engineering

Development of a system model to predict dynamic response of a rotational electromagnetic vibration energy harvester

MAX CHRISTENSEN
JONATHAN ULMESTRAND

CHALMERS
UNIVERSITY OF TECHNOLOGY

Department of Electrical Engineering
CHALMERS UNIVERSITY OF TECHNOLOGY
Gothenburg, Sweden 2021

Rotational vibration energy harvester
Development of a system model to predict dynamic response of a rotational electromagnetic vibration energy harvester
A Master's thesis in Electrical Engineering
MAX CHRISTENSEN
JONATHAN ULMESTRAND

Supervisor & examiner: Jonas Fredriksson, Department of Electrical Engineering
Supervisor: Andreas Vikerfors, ReVibe Energy

Department of Electrical Engineering
Chalmers University of Technology
SE-412 96 Gothenburg
Telephone +46 31 772 10 00

Cover: CAD model of the prototype designed during this master´s thesis

Gothenburg, Sweden 2021

Abstract

In industry today there is a need to supply wireless sensor networks with power without having to draw cables or replace batteries. For some situations, a solution to this can be found with the help of vibration energy harvesters. This technology harvest energy from ambient vibrations, and the majority of the harvesters today uses a spring-mass system. This project aims to explore the possibilities to in some cases instead, use an eccentric mass to convert the vibrations into electrical energy.

A mathematical model was developed and the system dynamics were analysed by simulating the model in MATLAB with different system parameters. Based on the observations from the simulation results, a prototype was designed and developed to verify the mathematical model. Results from the simulations and verification show that using an eccentric mass to harvest energy from ambient vibrations is feasible. The bandwidth of the rotational system exceeds the linear equivalent in some cases. Earlier research describe a necessity to apply an initial angular velocity in order to achieve maximum power output. This is viewed as a big challenge to overcome within the development of rotational vibration energy harvesters. The simulations show however, that in some specific cases the system could operate without initial energy.

Keywords: Energy harvesting, vibration energy harvesting, pendulum, eccentric mass, wireless sensor network

Preface

This project has been conducted at Chalmers University of Technology in collaboration with ReVibe Energy. ReVibe Energy is a technology start-up originating from SAAB Group and Chalmers University of Technology. Based on patented technology, the company is developing and marketing devices for converting vibrations into electricity to power industrial wireless sensor networks.

Firstly, we would like to express a big thanks to our supervisors, Jonas Fredriksson at Chalmers and Andreas Wikerfors at ReVibe Energy, who have provided knowledge and ideas for the project as well as energy and motivation for us personally.

We also want to thank Erik Godtman Kling for introducing us to this project, and you at ReVibe Energy who have provided knowledge and ideas to the thesis and a smile to our faces at the weekly meeting and the non stop jokes in Slack. Although we have never met some of you face to face, we have always felt welcomed and included. Thank you for providing us with equipment and work space at the facilities and especially thanks for teaching us everything there is to learn about temlor.

We would like to express a huge thanks to our dearest family and friends for all the moral support you have provided, everything from remote fikas or lunches, to highly rewarding and instructive conference trips, to late night conversations. You are an important factor behind us succeeding with this thesis, especially during the times of a pandemic.

Lastly we would like to thank each other for keeping up the energy and always providing new and exiting ideas. The quality of this thesis would not have been nearly as high without you. A huge thanks from me Jonathan/Max to you Max/Jonathan.

Max Christensen and Jonathan Ulmestrand, Gothenburg, June 2021

Ett intressant fall, på det hela taget - Ture Sventon

Contents

1

Introduction

In industry today there is a need to supply wireless sensor networks (WSN) with power without having to draw cables or replace batteries. A solution to this is implementation of vibration energy harvesters. This technology harvest energy from ambient vibrations, and the majority of the harvesters today uses a spring-mass system. This project aims to explore the possibilities to in some cases instead, use an eccentric mass to convert the vibrations into electrical energy.

1.1 Background

Within this section the interest in the technology is presented along with some earlier research conducted on the field. Lastly, a previous study is presented that, similar to this thesis, aims at researching the possibilities with a rotational vibration energy harvester (VEH).

1.1.1 The industry's and society's interest in VEHs

A big part of the industry today utilises machines and large equipment in their operations. These machines and equipment require maintenance and service to function for longer periods. To facilitate the maintenance there is an increased interest to measure the status and conditions including wear on bearings, irregularities in noise, temperatures and humidity [1, 2]. Implementing WSN is becoming more and more common, to measure and monitor the condition of this equipment. With the information from the WSN, it is possible to maximise the equipment lifetime, whilst minimising downtime and maintenance-related accidents. This generates a higher degree of utilisation of the resources. Another benefit is that accidents can be avoided which leads to an increased safety towards humans that operate nearby the equipment [2].

A big challenge with the implementation of WSN is however the requirement of a power supply. Today the power situation is mainly solved by using primary or secondary batteries [3]. This requires a high level of maintenance to ensure that the system can operate as desired. The lifetime of the sensor nodes usually depends on the energy capacity of the batteries, so to prolong the lifetime of the sensor, another power source is needed. Energy harvesting has recently attracted a lot of attention as a technology that, in some applications, can solve the problems that battery-powered sensor nodes

have [1]. This technology harvests energy from the ambient environment, such as heat, electromagnetic waves or vibrations [4].

The majority of the vibration energy harvester (VEH) designs have been based on a resonant single degree of freedom (DOF) mass-spring-damper system (see Figure 1.1). This kind of system has a single specific operating frequency that is dependent on the stiffness of the spring, resulting in the disadvantage that every VEH has to be designed to operate at a specific frequency with a small bandwidth. If the environment vibrations deviate from this operating frequency the output power from the system is greatly reduced if not non-existent [5]. To resolve this problem, it was suggested to examine the possibility to use an eccentric rotating mass that converts the vibrations into a rotational movement, which in turn is converted into electrical energy.

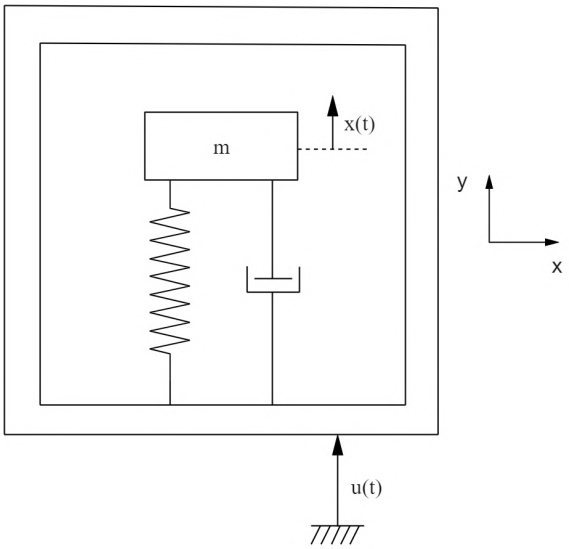

Figure 1.1: Illustration of a single degree mass-spring-damper system

The previous development within the field of rotating energy harvesters is limited, so this master's thesis aims to further examine and develop the possibilities to harvest energy from vibrations through an eccentric rotating mass.

1.1.2 Previous development within the vibration harvesting technology

Along with the growing interest for WSN [2], the attention on vibration energy harvesting applications have increased a lot the last few decades [6]. There are three different principles that traditionally are used to transduce ambient vibrations into electrical energy, piezoelectric, electrostatic and electromagnetic [7–9]. Piezoelectric VEHs utilises the vibrational energy to deform a piezoelectric material which generates a voltage when stressed. The electrostatic principle uses the vibrations to pull apart and achieve a displacement between two plates of a charged capacitor, which generates an alternating voltage. Electromagnetic transducers utilises the vibrations to create a relative movement between a permanent magnet and a coil to induce a voltage.

The standard linear products can produce output power in the range of 0.5-200 mW [10] and operate on vibrations with frequencies between 10 Hz and 150 Hz and with accelerations between 0.05 g up to 10 g. An example from [11], is the model D energy harvester with an operating frequency of 62.5 Hz which is exited by sine vibrations with an amplitude of 1 g. This harvester has 50 % of maximum power output or higher over a resistive load of 1000 Ω within an area with a bandwidth of 3 Hz.

The majority of the VEHs investigated during the literature study is based on a resonant single DOF mass-spring-damper system. The principle of transducing vibrational energy into electricity through an eccentric mass is less explored. One of the most common technologies based on the rotational VEH principle is however to utilise the energy from human motions. The Seiko watch [12] is an example of an application with this technology. The watch translates the motion of a human arm into a rotational motion that is converted into electrical energy that charges the watch battery. This system is capable to generate typically 5 μW with a maximum of up to 1 mW under certain conditions.

Although the principle of the Seiko watch is similar to the one suggested for this project, human motions will generate different vibrations than machine powered applications. The frequency of human motions usually ranges from 1-30 Hz whereas machine powered vibrations can range from 5 to several thousand Hz [13, 14]. The human motions are also usually random, while industrial vibrations are more periodic [15].

Literature within the field of rotating vibration harvesters has been sparse during literature searches for this project. However, the dynamics of a mathematical pendulum is a subject that has been studied for centuries. It has been studied by pioneer physicists like Galileo observing the period time of swinging pendulums as well as more recent studies seen in [16–22], among others.

1.1.3 Previous development of rotational vibration energy harvester

One promising study within the field of rotational vibration energy harvester is conducted by Spreemann et al. in [23], also reviewed by Spreemann and Manoli in [3]. The study cover modelling and simulation of two non-resonant conversion mechanisms as well as implementation and verification through a fine-mechanical power generator prototype. The developed prototype with a volume of 1.5 cm^3, generate a power of 0.4-3 mW for vibrations with an amplitude of 100 μm and frequencies ranging from 30 to 80 Hz. The model is compared to other similar models in several papers, see e.g. [24, 25], and is presented as one of the most promising models in the aspects of maximum output power density.

The significant difference between the two simulated models in the study [23], mentioned above, is the size of the harvester and mostly the pendulum length compared to the vibration amplitude. The fine-mechanical system had a pendulum length much longer than the vibration amplitude, while the Microelectromechanical system (MEMS) mechanism had a pendulum with the length in the same order of magnitude as the vibration amplitude. The two different mechanisms showed very different character-

istics in power generation. The MEMS mechanism did not require any initial angular velocity but generated power from the vibration energy alone. The fine-mechanical system on the other hand did not move into full rotations by the vibration alone, but external energy had to be added to initiate the rotations. After an initial angular velocity, same as the vibrations, have been applied the pendulum rotated with an angular velocity equal to the frequency of the vibrations.

One of the biggest possibilities with this conversion method of a VEH is according to [23] that the power generation is effective for a wide frequency band. Other mentioned advantages with this system compared to a resonant VEH, is that the transducer has two degrees of freedom for conversion of energy and that higher and lower modes of the vibration will be converted simultaneously.

Spreemann and Manoli [3] mention some challenges which are the main reasons why they choose to not focus on developing this concept further. Their biggest argument of exclusion is the necessity to apply an initial angular rate. This includes several complications and vulnerabilities to the system. The system requires an initial energy source to be able to accelerate, but if the energy source is empty, the pendulum will not be able to harvest the energy from the vibrations, and the system is no longer self-sufficient. To be able to match the frequency of the vibrations, a sensor is needed to read the vibrations, which additionally requires initial energy. They also mention that the generator that transduces the rotational energy into electricity, needs to work as a motor, to be able to apply the initial angular rate. This may limit the output energy in the generator. Another challenge they mention is that the system is sensitive to quick changes in the input vibration frequency, for example, gearshift in a car.

1.2 Aim

This project has aimed to develop a system model for a VEH that can harvest energy from vibrations from the environment with the use of a rotating eccentric mass. The rotation will in turn generate electricity by the use of induction. In order to specify the goal further, three research questions have posed. These questions has served as guidelines to help steer the investigation.

- In what situations is a rotational VEH preferable to a linear one, based on power extraction and frequency bandwidth?
  - If the rotational design is to be of any practical use, situations where this design can outperform the current mass-spring systems need to be found and characterised.
- What are the key characteristics that explain the differences in the performance of the linear and the rotational principle of energy harvesting?
  - If the previous question revealed that the rotational design could be beneficial, the differences between the different designs need to be identified. To help with this it needs to be investigated why the two different types of har-

vester perform differently with respect to minimum vibration acceleration, energy losses and frequency range.

- How can a rotational VEH be designed to maximise power extraction and frequency bandwidth?
  - To be able to answer this question the dynamics of the rotational mass need to be investigated. This means that the parameters that govern the key dynamics of the pendulum and how they can be tuned for maximum efficiency needed to be found.

1.3 Limitations

One simplification of the problem has been to use a stepper motor as a generator to convert the mechanical energy from the rotations into electrical energy. This has eliminated the need to design and implement this part and leave more time for analysis of the entire system. Since the efficiency and other relevant data for the motor is known by calculations or measurements, a model for the entire system can be updated to fit transducers with different properties.

There is a problem described Spreemann and Manoli [3] where the pendulum, for certain sets of parameters, needs to be accelerated from a standstill into a specific set of states. This is so the system can rotate on its own and not oscillate. To solve this problem it requires that an external driving torque can be applied to the rotational axis to steer the motion of the pendulum into a desired mode. Designing an external system that can accelerate the pendulum up to the desired frequency, has not been within the focus of this project, to make it more feasible with respect to time limitations.

This thesis generally focus on the mechanical dynamics of the pendulum system, and how to maximise its kinetic energy based on different vibrations. The electrical aspects of vibration energy harvesting is mostly disregarded as a lot of research in this field already has been conducted.

1.4 Outline of the thesis

This thesis is divided into seven chapters, where chapter 2 to 5 consists of the method and results of the project and the last two clarifies the discussion, conclusions and recommendations.

Chapter 2 describes how theory is applied to the rotational vibration energy harvester technology to achieve an accurate mathematical model of the system.

In chapter 3, the model is analysed by simulating the model in MATLAB with different system parameters.

Based on the observations from the simulation results, chapter 4 describes the prototype development and design, which in chapter 5 is used for verification of the model.

The discussion can be found in chapter 6 and finally the conclusions and recommendations for further research in chapter 7.

2

Modelling of the transducer system

To be able to simulate the system, a mathematical model of the system was needed. This model was expressed as a differential equation (see equation 2.12) that was calculated using Newton's laws. In order to reason about how a generator might affect the dynamics of the pendulum, a simple model of a DC-generator was calculated with the motivation that these effects would be similar for other types of electro-mechanical generators. Lastly, some reasoning about the energy input and output of the system has been made.

2.1 The mechanical subsystem

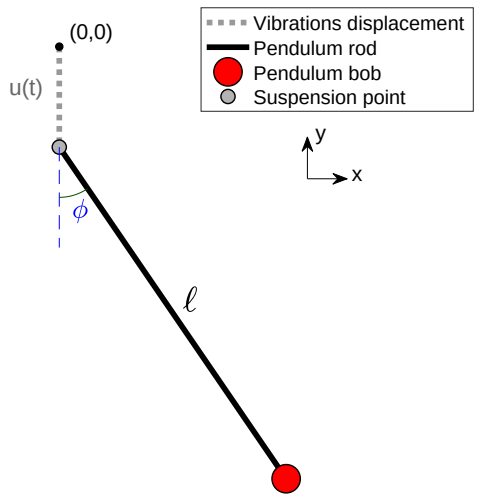

Figure 2.1: A model of a pendulum with a vertically oscillating suspension point

A mathematical pendulum, shown in Figure 2.1, can be described as a bob with mass m at the end of a massless rod with length ℓ that is hanging from a pivot point. This allows the pendulum to swing around the suspension point. The mass of the pendulum bob is considered small enough that the movement of the pendulum will not affect the vibrations. Any friction or other damping acting on the pendulum is modelled as viscous damping. Using Newton's laws, the angular acceleration of the pendulum can be

written as a differential equation:

$$\begin{aligned}\ddot{\phi} = & f(\phi, \dot{\phi}) = \frac{1}{J}\left(T_{\mathrm{d}}(\dot{\phi}) + T_{\mathrm{g}}(\phi) + T_{\mathrm{v}}(\phi)\right) = \\ = & \ddot{\phi}_{\mathrm{d}} + \ddot{\phi}_{\mathrm{g}} + \ddot{\phi}_{\mathrm{v}}\end{aligned} \tag{2.1}$$

where ϕ is the angle and $J = m\ell^2$ is the inertia of the pendulum, T_{d}, T_{g} and T_{v} are the torques exerted from the viscous damping, gravity and the vibrations onto the pendulum and $\ddot{\phi}_{\mathrm{d}}$, $\ddot{\phi}_{\mathrm{g}}$ and $\ddot{\phi}_{\mathrm{v}}$ are their corresponding angular accelerations. These accelerations can be described in more detail.

The damping torque T_{d} can be modelled as a viscous damping, meaning that a constant, γ_T, multiplied with the angular velocity results in the torque applied from the damping. The transformation γ from angular velocity to the angular acceleration by the damping can then be written as

$$\ddot{\phi}_{\mathrm{d}} = \frac{T_{\mathrm{d}}}{J} = -\frac{\gamma_T \dot{\phi}}{J} = -\gamma\dot{\phi}. \tag{2.2}$$

The constant γ is henceforth referred to as the *damping constant*.

The gravity will affect the pendulum by exerting a downward force on the pendulum bob. This will result in a torque around the suspension point of the pendulum which will result in an angular acceleration.

$$\ddot{\phi}_{\mathrm{g}} = \frac{T_{\mathrm{g}}}{J} = \frac{mg\ell\sin(\phi)}{m\ell^2} = \frac{g}{\ell}\sin(\phi) \tag{2.3}$$

Combining equation 2.1 with equations 2.2 and 2.3, the total acceleration of the pendulum becomes

$$\ddot{\phi} = -\gamma\dot{\phi} - \frac{g}{\ell}\sin(\phi) + \ddot{\phi}_{\mathrm{v}}. \tag{2.4}$$

If the position of the suspension point of the pendulum oscillates vertically by

$$u(t) = -\frac{A_y}{\omega^2}\cos(\omega t) \tag{2.5}$$

were, A_y is the amplitude of the acceleration and ω is the frequency of the vibrations. The corresponding acceleration of this oscillation translates to the angular acceleration of the pendulum according to

$$\ddot{\phi}_{\mathrm{v}} = \frac{T_{\mathrm{v}}}{J} = \frac{m\ddot{u}(t)\ell\sin(\phi)}{m\ell^2} = \frac{1}{\ell}\ddot{u}(t)\sin(\phi). \tag{2.6}$$

Combining equation 2.6 with equation 2.4 it is clear that the pendulum dynamics can be described by

$$\begin{aligned}\ddot{\phi} = & -\gamma\dot{\phi} - \frac{g}{\ell}\sin(\phi) + \frac{1}{\ell}\ddot{u}(t)\sin(\phi) = \\ & -\gamma\dot{\phi} - \frac{1}{\ell}\left(g\sin(\phi) - A_y\cos(\omega t)\sin(\phi)\right)\end{aligned} \tag{2.7}$$

In a similar way, a system with a suspension point that oscillates horizontally according to

$$v(t) = \frac{A_x}{\omega^2}\sin(\omega t) \tag{2.8}$$

with the acceleration A_x can be described by modifying equation 2.4 in the following way:

$$\begin{aligned}\ddot{\phi} = &-\gamma\dot{\phi} - \frac{g}{\ell}g\sin(\phi) + \frac{1}{\ell}\ddot{v}(t)\cos(\phi) = \\ &-\gamma\dot{\phi} - \frac{1}{\ell}\left(g\sin(\phi) + A_x\sin(\omega t)\cos(\phi)\right).\end{aligned} \tag{2.9}$$

With both vertical and horizontal oscillations of the suspension point, the system equation becomes

$$\begin{aligned}\ddot{\phi} = &-\gamma\dot{\phi} - \frac{1}{\ell}\left(g\sin(\phi) - \ddot{u}(t)\sin(\phi) - \ddot{v}(t)\cos(\phi)\right) = \\ &-\gamma\dot{\phi} - \frac{1}{\ell}\left(g\sin(\phi) - A_y\cos(\omega t)\sin(\phi) + A_x\sin(\omega t)\cos(\phi)\right)\end{aligned} \tag{2.10}$$

If the vibrations are circular, one can describe the system as in Figure 2.2 by considering

$$A = A_y = A_x. \tag{2.11}$$

Equation 2.10 can then be simplified into

$$\ddot{\phi} = -\gamma\dot{\phi} - \frac{1}{\ell}\left(g\sin(\phi) + A\sin(\omega t - \phi)\right). \tag{2.12}$$

The systems described by equations 2.10 and 2.12 cannot be analytically solved, so simulation must involve solving these equations numerically.

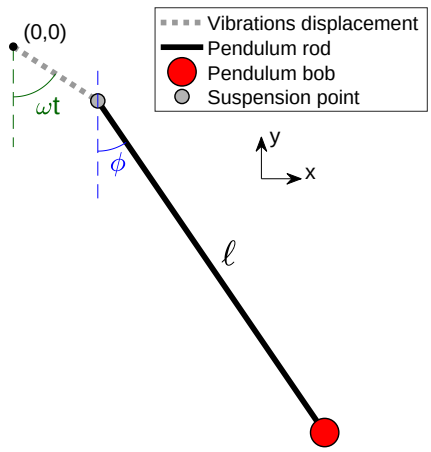

Figure 2.2: Pendulum with a suspension point that moves in a circular trajectory

2.2 The generator subsystem

The damping constant γ describes the friction and heat losses from both the mechanical and the electrical subsystems and the characteristics of the generator. The damping constant can then be divided into a mechanical part γ_f and an electrical part γ_E as:

$$\gamma = \gamma_f + \gamma_E. \tag{2.13}$$

While the mechanical friction is considered constant, the damping produced by the generator can be estimated in more detail. A simple permanent DC motor model is chosen because of its simplicity and because most generators use the same principles to operate. The relation between the angular velocity $\dot{\phi}$ of the mechanical axis and the generated electric voltage V for an ideal DC generator is described by

$$V = KB\dot{\phi} \tag{2.14}$$

where K is a constant dependent on the generator design and B is the magnetic flux from the magnets. For an ideal generator, the relation between the current I and the developed damping torque T, shown in equation 2.15, is the same as between the angular velocity and and the generated voltage in equation 2.14.

$$T = KBI \tag{2.15}$$

Combining these two equations together with Ohms law $V = RI$ where R is the total resistance in the circuit, one can find an expression for the damping torque expressed as a function of the angular velocity.

$$T = \frac{(KB)^2}{R}\dot{\phi} \tag{2.16}$$

Dividing the torque by the inertia of the pendulum (J) yields the acceleration produced by the damping. The component γ_E of the damping constant γ can then be written as

$$\gamma_E\dot{\phi} = \frac{(KB)^2}{RJ}\dot{\phi} = \frac{T}{J} \tag{2.17}$$

2.3 Energy in rotations

The rotational kinetic energy of the pendulum can be expressed as

$$E_{\text{rot}} = \frac{1}{2}J\dot{\phi}^2 \tag{2.18}$$

meaning that in order to maximize the possible energy output, the angular velocity need to be maximized. Since the electrical power produced over a resistive load R_L can be expressed as

$$P_{\text{el}} = V_{R_L}I \tag{2.19}$$

where V_{R_L} is the voltage over the load. This means according to the proportional relation between electrical current and damping torque in equation 2.15, that the damping

torque will then increase proportional to the current.

The energy input and output of the pendulum subsystem can be viewed as the three torque components in equation 2.1. Here the torque from the vibrations is what is giving energy to the pendulum. The torque applied from gravity will not change the energy levels over time more than that it will store and release potential energy as the pendulum bob moves vertically. This means that the energy that is taken from the system is taken from friction and the reverse torque produced by the induced current in the transducer.

Looking deeper in to equations 2.10 and 2.12 the maximum power transfer with the largest possible damping constant can be found when the phase of the pendulum lies 90° behind the vibrations.

3

Analysis of the transducer system

In order to examine how the system would respond for different parameter values, equations 2.12 and 2.9 were simulated by solving the differential equations numerically with the ODE45 function in MATLAB. The simulations enabled efficient analysis and testing of the system as several of the different parameters could be run at once. The purpose of the simulations was to examine how the system would respond for different parameter values in order to maximise the harvested energy as well as identifying any obstacles that might lay in the way of this goal. If different initial values led to different steady state trajectories, or attractors, these sets of initial values, or basins of attraction, were also identified.

The simulations have shown that the pendulum can exhibit several different types of trajectories depending on the different parameter values (see Figure 3.1). These trajectories include rotations of the same frequency as the vibrations, rotations with half the frequency of the vibrations and oscillations around the downward hanging position. The pendulum can also move in trajectories described as chaotic which in this thesis means that the pendulum switches between rotations and oscillations. This can happen for both linear and rotational vibrations, labelled as "Single axis chaos" and "Rotating chaos" respectively in Figure 3.1. No more formal definition of chaotic movement is made in this report.

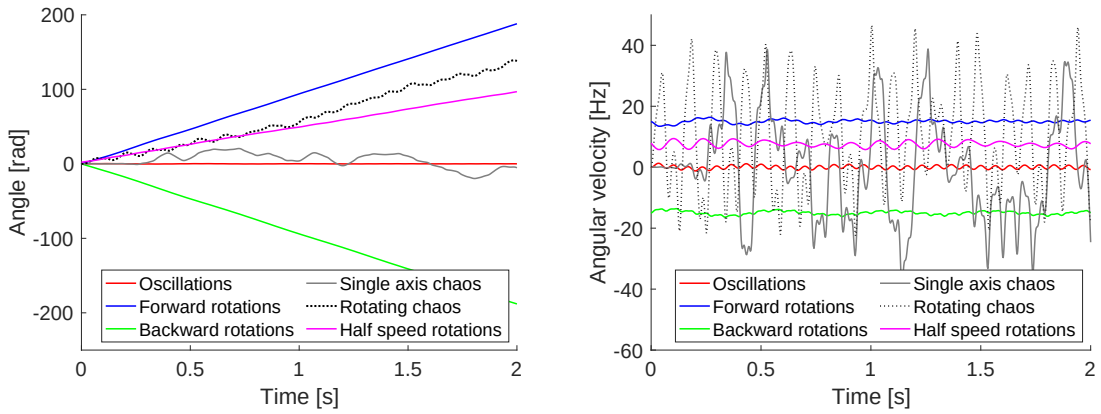

(a) Angles over time

(b) Velocities over time

Figure 3.1: Examples of different types of trajectories that the system can exhibit.

The initial parameter values for these simulations, henceforth referred as the *nominal system*, can be seen in Table 3.1. They were mostly chosen as what was considered reasonable values for a possible prototype with consideration taken for what could be tested on available equipment. The vibration amplitude and frequency were chosen from data from what could be a possible real world application for this type of harvester [26]. Parameter sweeps were then performed by changing a single parameter and plotting series of plots with mean angular velocity plotted as a function of initial conditions for the different parameter values.

These simulations were performed for both rotational vibrations when the suspension point moves in a circle and, for some tests, vibrations along one axis. The reason for investigating the rotational vibrations more is that the linear vibrations are more investigated in the literature [16–22]. In the case with vibrations along one axis, the initial damping constant was halved in order to keep similar movements of the pendulum as starting points for the simulations. This was because there is less energy in linear vibrations compared to rotating ones of the same frequency and amplitude.

Table 3.1: Initial parameter values for the simulations.

Pendulum rod length (ℓ)	50 [mm]
Pendulum bob mass (m)	27 [g]
damping constant (γ)	2 [s^{-1}] (rotating vibrations)
damping constant (γ)	1 [s^{-1}] (linear vibrations)
Vibration acceleration (A)	2 [g]
Vibration frequency (ω)	15 [Hz]

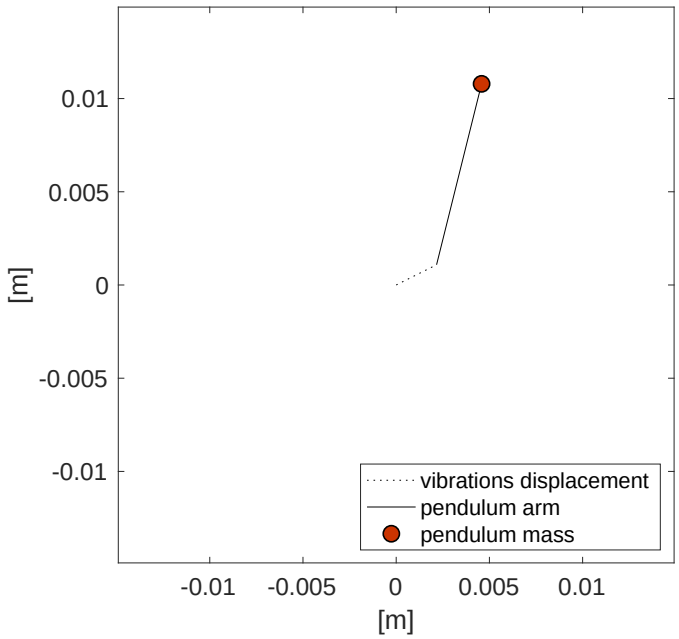

Figure 3.2: Example of a single time step of the simple pendulum simulation with vibrations displacement, pendulum rod and pendulum mass.

To begin with, the system model described by equation 2.10 was simulated in MATLAB and a simple plot of the position of the pendulum relative to the vibrations was animated. This was in order to get a simple and clear view of how the system trajectories would develop with different parameter values. An example of how the simulation looks can be seen in Figure 3.2. These animations of single trajectories of the system have been used throughout the tests as a way of verifying the results from other simulations.

In order to test the model for a larger number of trajectories, the angular velocity and the angle were plotted against each other and separately over time for a range of initial angles and angular velocities. These plots were used both as ways of showing the different types of pendulum movements and as ways to estimate how long time the simulation needed to run in order for the trajectories to their respective attractors.

3.1 The nominal system

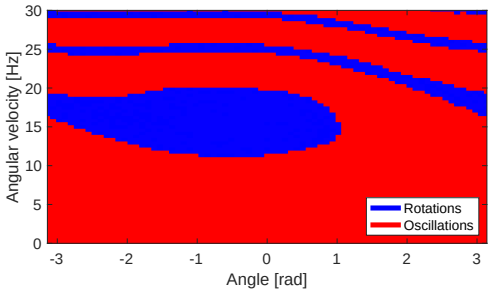

(a) Basin of attraction

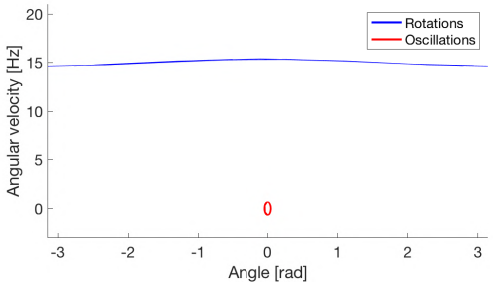

(b) Trajectories over last three periods of simulation

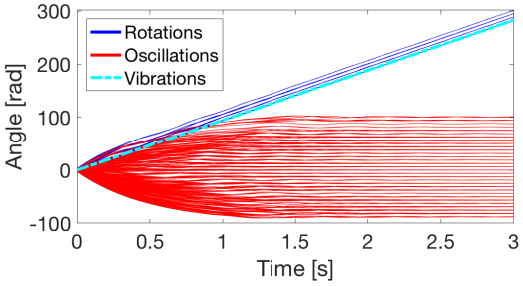

(c) Angular velocities over time

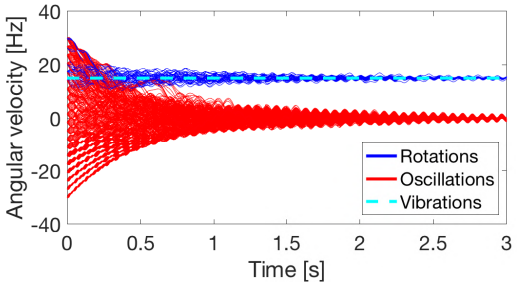

(d) Angles over time

Figure 3.3: Simulation results from simulating multiple trajectories with rotating vibrations and different initial values. Different colors indicate different attractors.

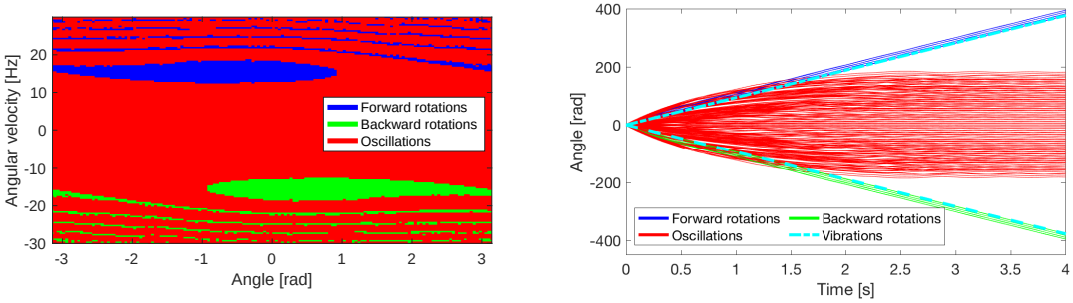

(a) Basin of attraction

(b) Angles over time

Figure 3.4: Simulation results from simulating multiple trajectories with linear vibrations and different initial values. Blue, red and greed trajectories correspond to different attractors.

One conclusion from the single trajectory plot was that if the system landed in rotating or oscillating trajectories depended heavily on the initial angle and velocity. To get a better understanding on what initial conditions lead to what kind of behaviour the mean velocity for the simulations was plotted as a function of the initial values. The first part of the simulations was discarded in order to let the results converge to their resulting trajectories.

When examining the different plots over the angle and angular velocity seen in Figures 3.3 and 3.4, the colors show three stable types of trajectories for the nominal system with parameters shown in Table 3.1. Two with full rotations, one in each direction, and one with oscillations around the downward hanging position. The system rotates in only one direction when subjected to rotating vibrations and in two directions when subjected to linear vibrations. Since the kinetic energy of the system scales with the square of the angular velocity it can also be concluded that the full rotations are a more attractive mode since it has the higher mean angular velocity.

3.2 Changing the damping constant

One parameter that could potentially affect the system performance was the damping constant. Simulations were therefore ran when the damping constant was changed while the other parameters were kept as the nominal system parameters shown in Table 3.1.

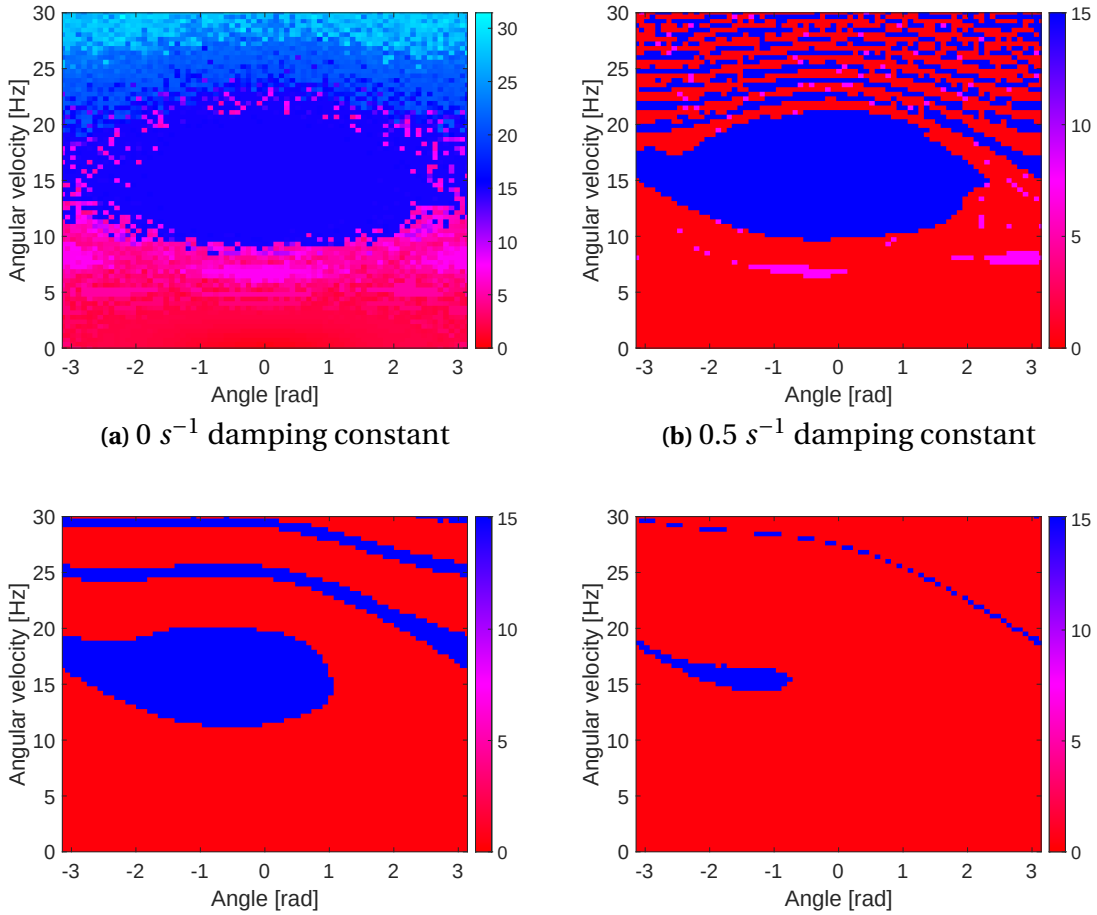

(a) 0 s^{-1} damping constant

(b) 0.5 s^{-1} damping constant

(c) 2 s^{-1} damping constant

(d) 4 s^{-1} damping constant

Figure 3.5: Color coded mean velocity as a function of initial angle and angular velocity.

When the damping constant is increased the basin of attraction for rotating solutions decrease in size until all the trajectories end in oscillations at a damping constant of 5 s^{-1}. When the constant is decreased the basin of attraction for rotations increases in size until the damping is set to zero meaning a system without any friction or torque back from the generator. The system is not tested for negative damping. When the constant reaches 0.7 s^{-1} for the nominal system, trajectories with half the angular velocity appears. Plots from simulations with different damping constants can be seen in Figure 3.5.

3.3 Gravity dependence

One limitation of the plots generated from the tests is that because of the gravity affecting the pendulum, they are also dependent on the initial angle of the vibrations. For a given initial pendulum angle, the vibrations could start at any angle. This could potentially make the basin of attraction change shape depending on the initial angle of

the vibrations. To investigate how the gravity affects the system, the basin of attraction was plotted for different initial vibration angles.

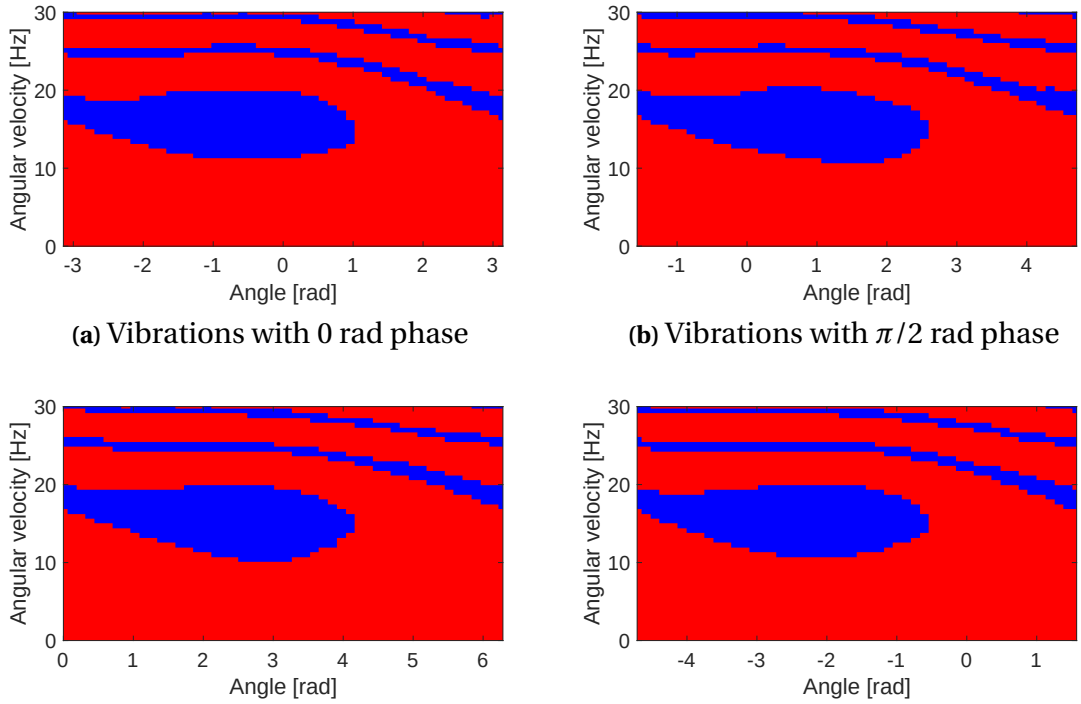

(a) Vibrations with 0 rad phase

(b) Vibrations with $\pi/2$ rad phase

(c) Vibrations with π rad phase

(d) Vibrations with -$\pi/2$ rad phase

Figure 3.6: Basin of attraction for different initial phase of the vibrations.

In equation 2.12, the maximum acceleration from the gravity can be calculated as g/ℓ and the maximum acceleration as A/ℓ. The vibration acceleration for the nominal system is $A = 2 \times g$ meaning that the gravity can stand for one third of the total driving acceleration applied to the pendulum. However the results seen in Figure 3.6 show that the shape of the basins of attraction for different initial vibration angles is mostly the same.

3.4 Chaotic motion

According to Spreemann et al. [23], the pendulum trajectories become chaotic if the pendulum rod length is of the same order of magnitude as the displacement of the vibrations. The nominal vibrations used in the simulations have a displacement of $A/\omega^2 = 2.2$ mm. When the length of the pendulum was changed to the same, the trajectories became chaotic. This type of behaviour of the system was further investigated as seen in Figure 3.7. Here all the tested trajectories with rotational vibrations and different initial conditions achieve net rotations when in this mode but the mean angular velocity is calculated as 10 Hz compared to the rotations 15 Hz. Linear vibrations does not give net rotations in this manner as seen by the difference in both angle and mean angular velocity in Figures 3.7 and 3.8. However, when investigating the RMS value of

the velocities in the linear and rotating case the two cases have 19 Hz and 18 Hz RMS value respectively.

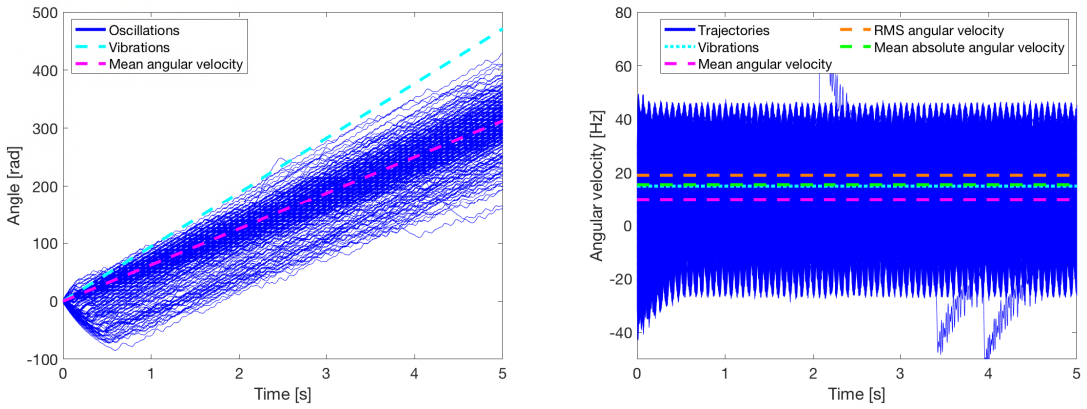

(a) Angles over time **(b)** Angular velocities over time

Figure 3.7: Simulations with rotating vibrations and with the parameters in Table 3.1 except for the pendulum rod length which is shortened to 2.2 mm.

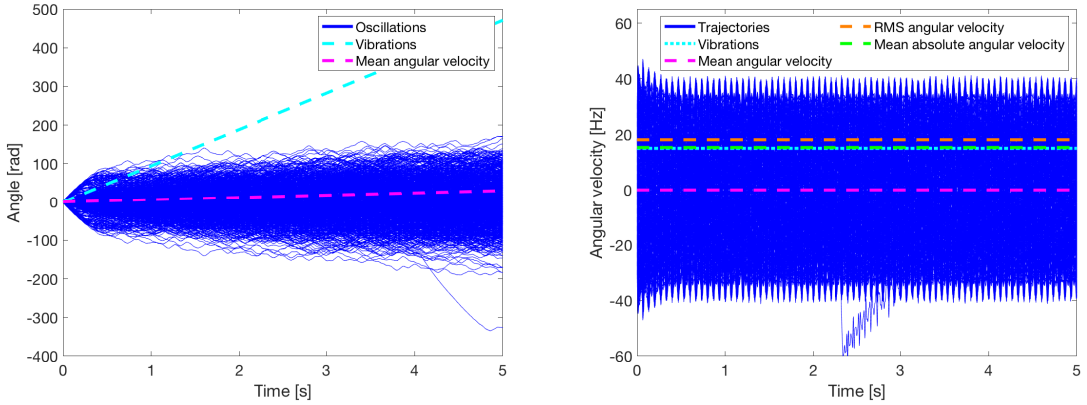

(a) Angles over time **(b)** Angular velocities over time

Figure 3.8: Simulations with linear vibrations and with the parameters in Table 3.1 except for the pendulum rod length which is shortened to 2.2 mm.

If for example an AC-generator is used where the mean output voltage would scale with the mean of the absolute value of the angular velocity of the pendulum, the direction of the rotations would be irrelevant. Calculating this average angular speed of the chaotic trajectories above result in an average angular speed of just above the vibrations at 15.3 Hz for the linear rotations and 15.5 Hz for the rotational vibrations.

Figure 3.9b shows how the chaotic system for linear vibrations depend on the initial values. The results show that all trajectories have a mean absolute angular velocity

that is similar to the vibration frequency. This can be compared to figure 3.9a where the same analysis for the nominal system can be seen.

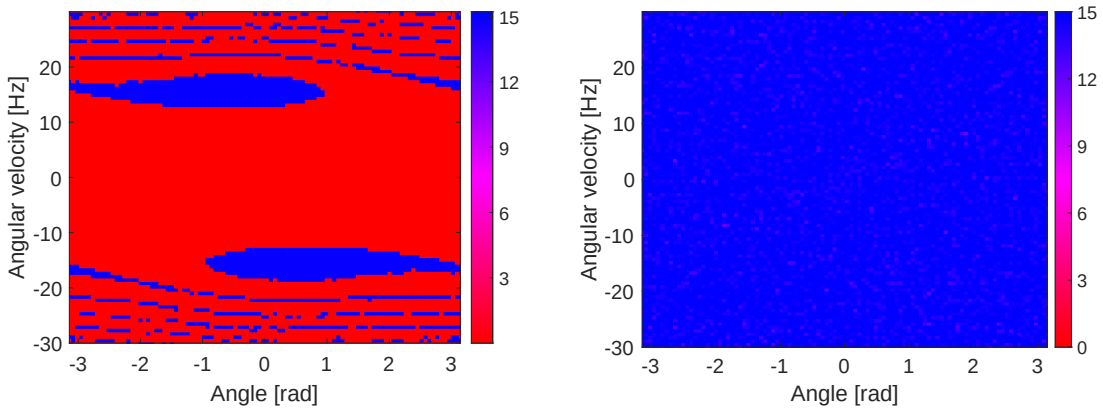

(a) Nominal system **(b)** Chaotic system

Figure 3.9: Color coded mean absolute velocities for different initial values for the nominal and the chaotic system with single-axis vibrations.

3.5 Bandwidth

Since one of the proposed benefits of a rotational design is that the system can handle vibrations of a larger bandwidth than the traditional single axis, resonant VEH can, simulations were performed in order to verify this. One problem with calculating the bandwidth for this system is that when the frequency of the vibrations changes, either the amplitude or the displacement or both has to change as well. This is because they depend on each other according to

$$A = \omega^2 d \tag{3.1}$$

where d is the displacement. To investigate the results of keeping either the displacement or the acceleration constant, both cases were simulated for different frequencies.

When investigating these cases, one upper and one lower limit was found. The upper limit was found when keeping the vibration acceleration constant and increasing the frequency. Here the basin of attraction for the rotating trajectories decreased until all initial states ended up in oscillations around the downwards hanging position. The last integer frequency with full rotations was found at 31 Hz. The lower bound was found when the displacement of the vibrations was kept constant and the frequency was lowered. Here the basin of attraction decreased as well until there only existed oscillations. The lowest integer frequency found with full rotations was at 7 Hz. The basin of attraction for these two frequencies can be seen in Figure 3.10.

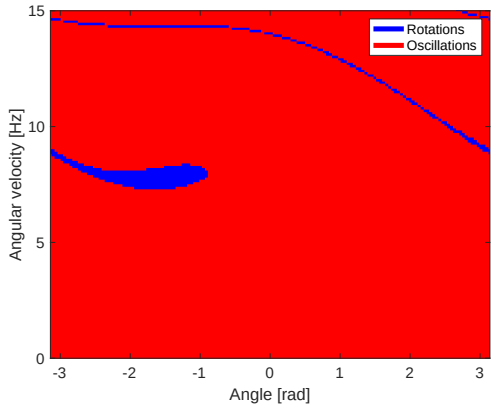

(a) Lower bound 7 Hz vibrations with a constant displacement of 2.2 mm.

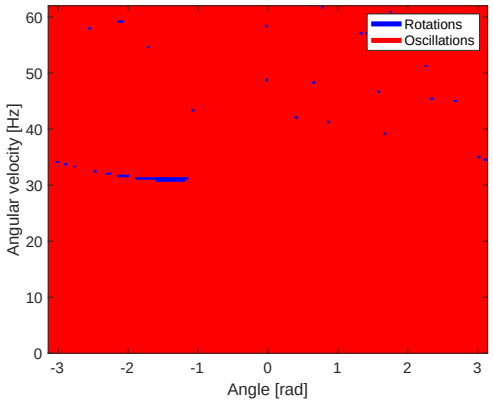

(b) Upper bound 31 Hz vibrations with a constant acceleration of 2 g.

Figure 3.10: Basin of attractions for last integer frequencies before all initial states result in oscillations.

When keeping the acceleration constant and decreasing the frequency, the basin of attraction grows until the oscillating trajectories disappear. At 5 Hz all the initial conditions lead to fully rotating solutions and at 3 Hz all the trajectories experience chaotic movement with net rotations with an angular velocity of 2 Hz (see Figure 3.11).

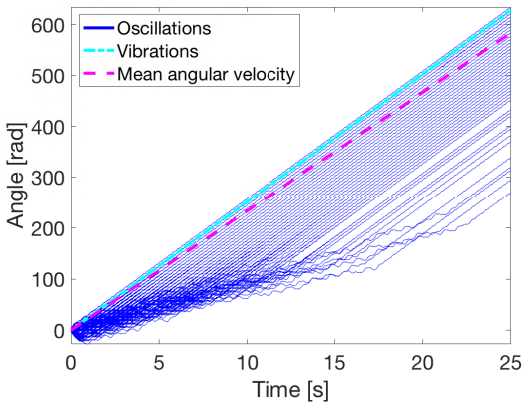

(a) Vibration frequency of 4 Hz

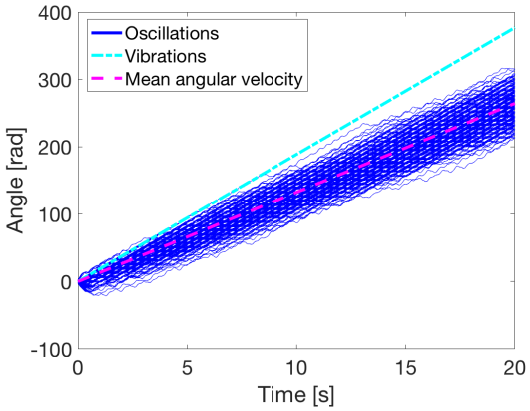

(b) Vibration frequency of 3 Hz

Figure 3.11: Pendulum angle from simulations with nominal system and constant vibration acceleration and decreasing vibration frequency and displacement.

Simulating when keeping the displacement constant and increasing the frequency also results in an increasing basin of attraction. The oscillating trajectories does however not disappear for the frequencies tested (<150 Hz).

To get a better understanding of how the different parameters affect the system in terms of the two states rotations or non-rotations (oscillations), simulations were run

where the damping was initially set low and then increased to a point where the rotations stopped to occur (see Figure 3.12). The highest damping that resulted in rotations for each set of parameters, and for at least one of the initial values, is represented by the lines. This means that below the limits there are cases where the system shows continuous rotations, and above the lines there are no initial value that resulted in rotations.

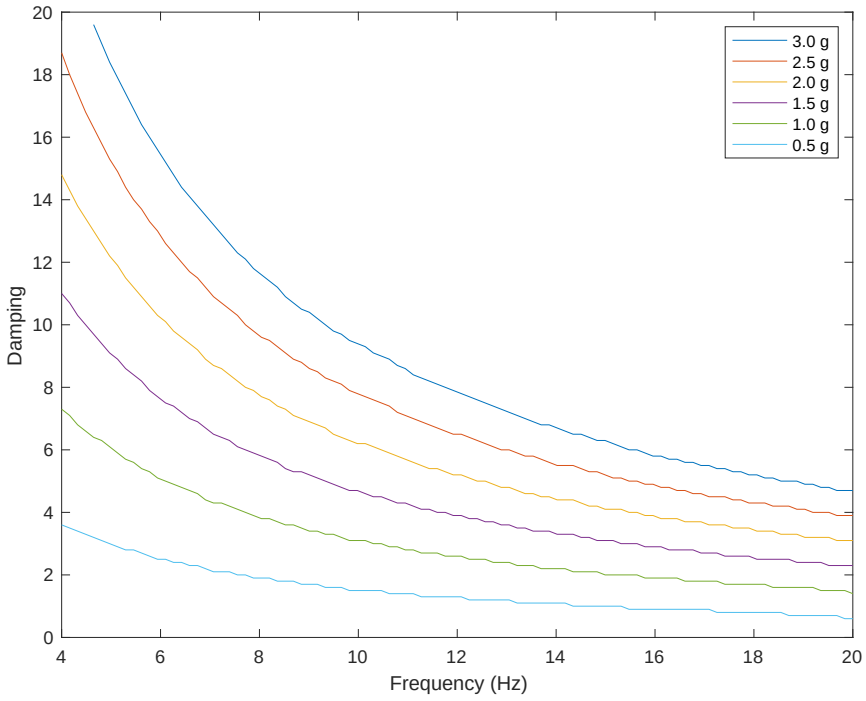

Figure 3.12: Parameter limits between regions where the initial conditions can result in continuous rotations (below the limits) and where all the initial conditions result in oscillations (above the limits).

3.6 Changes in vibration

Another aspect of the system's property to handle different vibrations is how it handles changes in vibration frequency while the pendulum is rotating. This property has been investigated by simulating the system for a specific frequency until the trajectories had settled close to the attractor. Then the frequency was changed by a discrete step.

When simulating the step change in frequency in Figure 3.13, it can be seen that the nominal system can handle step changes in vibration frequency of up to 3 Hz. This can be viewed when simulating a discrete change in frequency as two systems with different frequencies and using the final states for the first system as initial values for the second. If the trajectories from the first system are within the area of attraction of the second, the trajectories will settle in rotations for the new system.

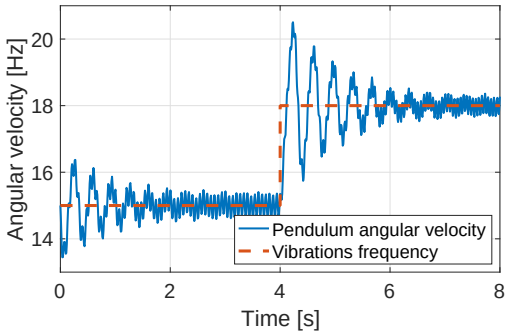

(a) Single trajectory with vibration increase of 3 rad/s

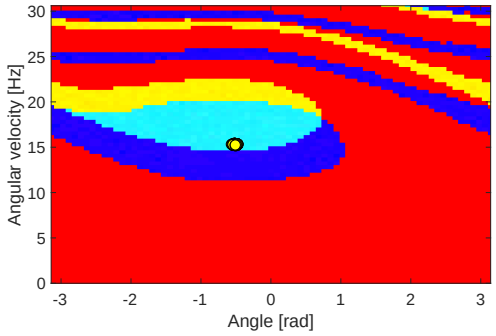

(b) Basin of attraction for systems with 15 and 18 Hz and system states (yellow dot) before frequency change.

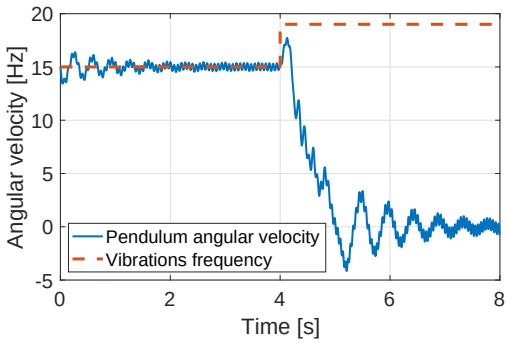

(c) Single trajectory with vibration increase of 4 rad/s

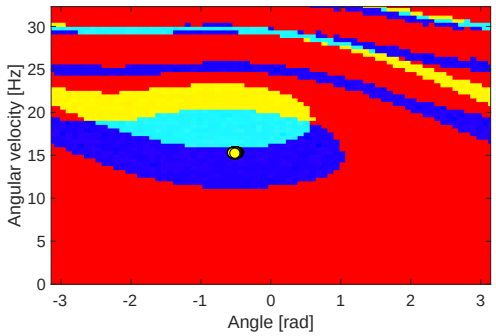

(d) Basin of attraction for systems with 15 and 19 Hz and system states (yellow dot) before frequency change.

Figure 3.13: Simulation results for the nominal system with frequency increases of 3 and 4 Hz during simulation.

4

Implementation through prototype design and development

To verify the mathematical model a physical test rig was designed (see Figure 4.1). With this rig the damping of the system, partly from parasitic loss and partly from the damping of the generator, could be measured and then used in the mathematical model. The test rig was designed to make it relatively simple to test and change different parameters, such as different pendulum lengths and generators.

The prototype can be divided into different subsystems: the pendulum that transduces the vibrations into rotations, the generator that converts the rotations into electricity and the fixture that enable these parts to work as intended.

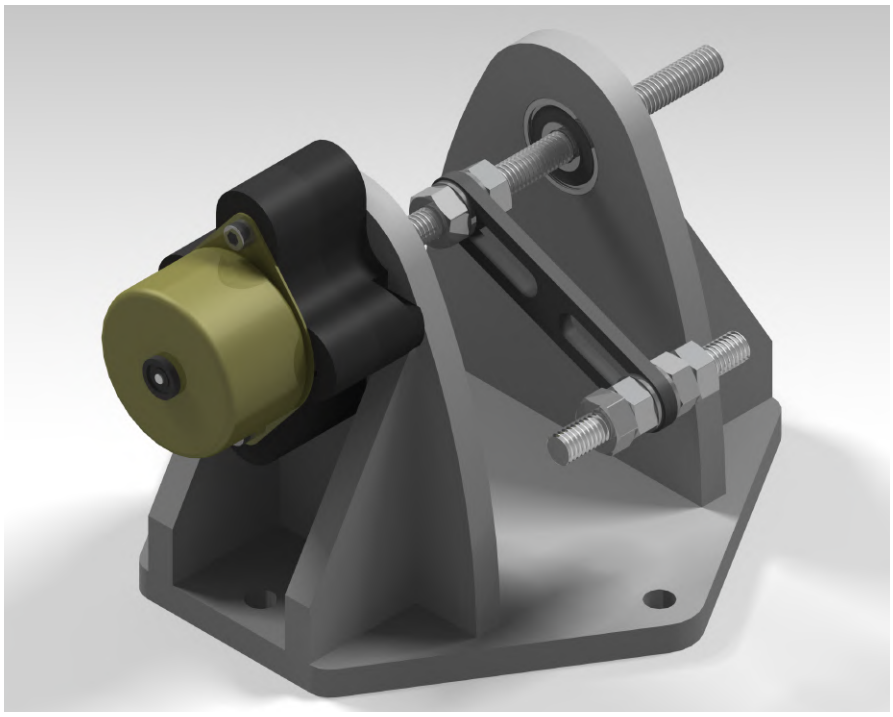

Figure 4.1: Rendering of the assembled prototype excluding the electronics subsystem.

4.1 The pendulum subsystem

The pendulum length was considered to have a big impact on the power output of the VEH. A maximum pendulum length was set to 50 mm, so that the sideways forces would not cause any damage on the testing equipment. It was desirable that the pendulum length and mass easily could be changed, for a flexible and easy verification of the different parameters. To simplify the calculations, the mass of the pendulum rod needed to be negligible compared to the mass of the pendulum bob.

When the critical requirements of the pendulum was identified a design was presented where the pendulum rod consisted of a plate with a groove and the bob consisted of a threaded bar and nuts, which could slide in the groove and get fixed at a desired pendulum length. A CAD model of the design was created in the software Catia, which enabled further requirement generation and improvements (see Figure 4.2). As the pendulum rod needed to have as low mass as possible, the material chosen for the rod was a polymer, based on its mechanical properties. The part was 3D-printed to finish the prototype as quickly as possible. With the M6 nuts attached, the minimum pendulum length was 13 mm and the maximum 50 mm.

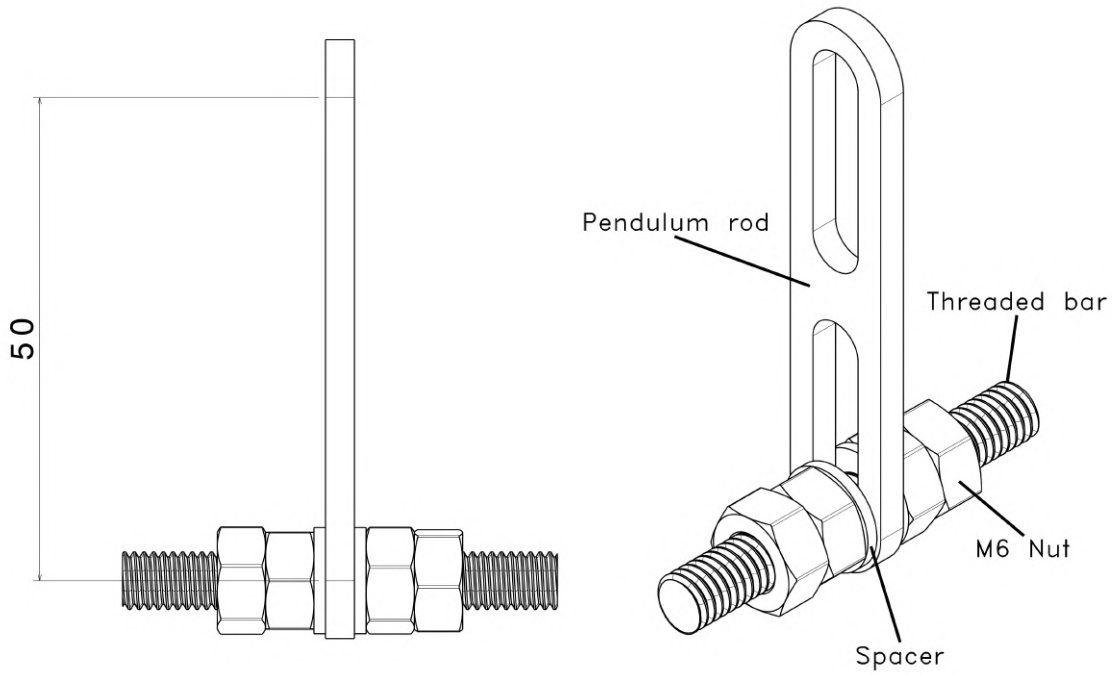

(a) The the maximum length of the pendulum was designed to 50 mm.

(b) The different parts of the pendulum subsystem.

Figure 4.2: The pendulum subsystem design.

4.2 The generator subsystem

As described in the limitations the conversion from rotations to electricity was limited to an off the shelf generator. From the simulations it was determined that the initial conditions have a huge impact on the possibilities for rotations, so angle and angular rate measuring was considered necessary. A unipolar permanent magnet stepper motor, listed in Table 4.1, was chosen as a generator to fulfil these requirements. It was a 6 lead, Premotec, ST32 UNI Stepper Motor with a step angle of 7.5° and four phases, meaning 12 voltage peaks per rotation on one phase [27].

Table 4.1: Technical data of the stepper motor [27]

ST32 UNI Stepper motor	
Type	Unipolar stepper motor
Step angle	7.5°
Resistance per phase (R_P)	120Ω
Inductance per phase (L_P)	$160mH$
Number of phases	4
Rotor inertia	$0.0026kgcm^2$

Figure 4.3 illustrates the six leads from the stepper motor, where red is common, and gray and yellow represent each phase.

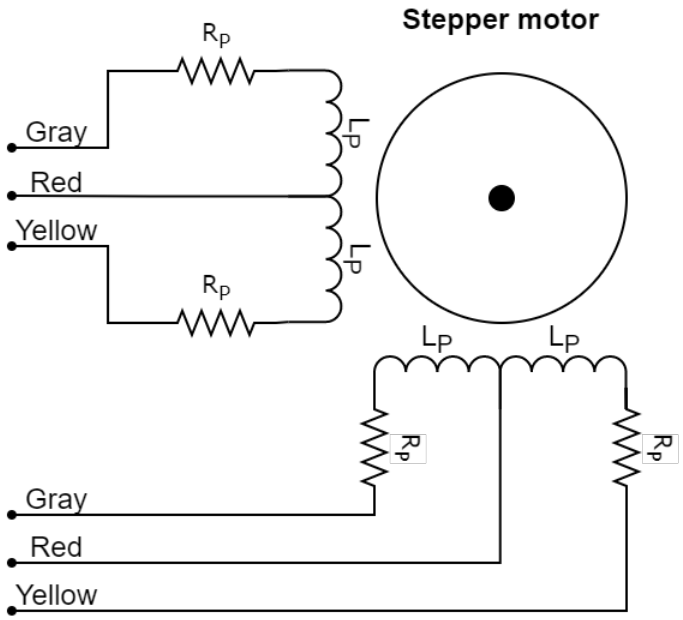

Figure 4.3: Circuit of the stepper motor with the six leads where R_P is the resistance and L_P is the inductance per phase.

4.3 The suspension subsystem

To reduce parasitical damping in the system, the generator was designed to be immediately fixed on the same rotation axis as the pendulum. A threaded bar was chosen for the axis to enable quick adjustments of parameters during verification.

The fixture of the test rig was designed accordingly with the requirements in Catia and then 3D-printed to quickly get a prototype ready for verification. It was designed so that two bearings could be interference fitted into the fixture, to enable rotation of the threaded bar. Holes in the bottom of the fixture enabled fixing in the shaker table with four screws, during verification.

A different stepper motor, than the final one, was originally used as a generator. The original stepper motor had different dimensions of the fixture holes than the final, which lead to that the new stepper motor could not be fixed in the original holes of the fixture. A connection part was modelled and then FDM 3D-printed to enable fixing of the new stepper motor.

5

Verification of the model and the design

To verify the quality of the mathematical model and to detect any unanticipated phenomena, the physical prototype was tested in real life environment. The verification phase consisted of three different tests, and has acted both as a proof-of-concept and a process to understand and develop the system further.

During the verification the verification phase monitoring of the system was performed by measuring the output voltage from the stepper motor with an Arduino Mega, if nothing else is stated. This enabled reading and storing voltage and elapsed time, which could be used in MATLAB to calculate the pendulum angle and angular velocity over time. The analog input port on the Arduino could only read positive voltages, while the voltage from one phase of the stepper motor was an alternating voltage with zero mean. The negative voltage values was therefore ignored which is why the figures illustrating voltages readings in this chapter only depicts positive voltages. The voltage was only read over one phase on the stepper motor due to that increasing the amount of analog readings for the Arduino decreased its sampling frequency.

To maximise the output power from the generator, the *maximum power transfer theorem* [28] states that the resistive load must equal the resistance in the generator. Figure 5.1 illustrates how the voltage V_{out} was read over a restisitve load R_L, that matched the resistance per phase R_P of 120Ω in the stepper motor, and where L_P is the phase inductance.

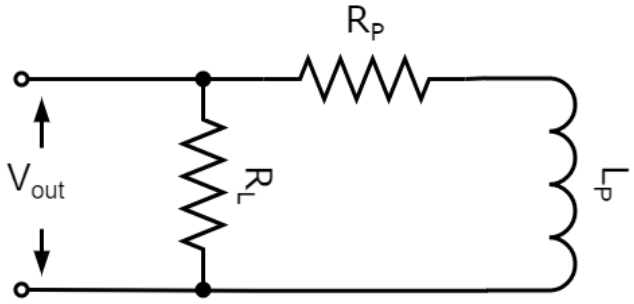

Figure 5.1: Schematic of how the reading of the phase was performed during verification.

As a way of verifying the model and obtaining a deeper understanding for the tests

the damping constant for the prototype was estimated a number of times. The results can be seen in Table 5.1 and the highest damping constant, along with the parameters for the tests were inserted in the mathematical model. The basin of attraction was simulated to better understand the results.

5.1 System test with spinning wheel

To be able to reason about the efficiency of this system, the output power was calculated. The pendulum was replaced with a homogeneous wooden wheel with a diameter of 98 mm, a thickness of 16 mm and a mass of 80 g. The voltage was continuously measured over a load resistance of 120 Ω when the wheel was accelerated by hand and then allowed to slow down by itself. The test was performed 4 times and the recorded voltage over time for the last test can be seen in Figure 5.2.

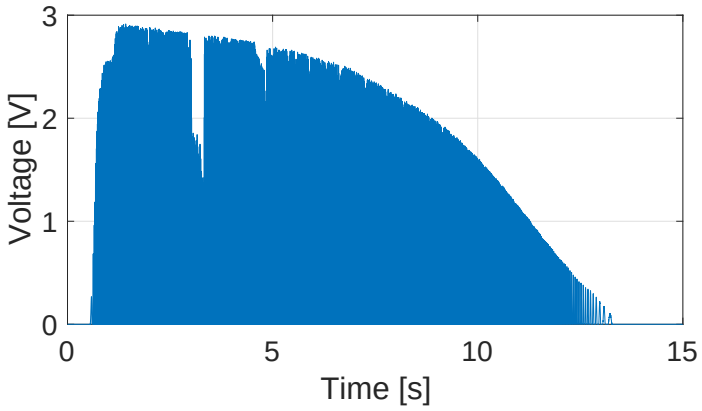

Figure 5.2: Recorded voltage for the test with a spinning wheel.

Since the output voltage from one phase of the stepper motor is a sinusoidal signal and therefore periodic, the frequency of the rotations can be estimated. This means that the peak output voltage from one phase can be plotted as a function of the frequency. This plot can be seen in Figure 5.3a. When the output voltage was found it then became possible to calculate the output power over the load resistance. This can be seen in Figure 5.3b. These plots are from the fourth test.

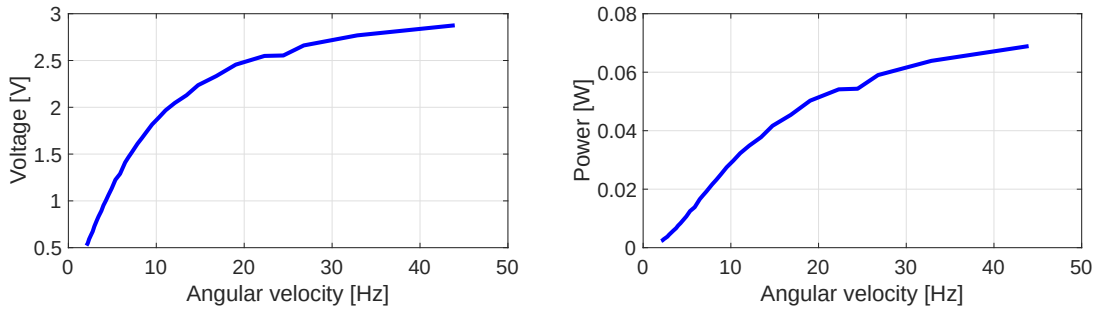

(a) Voltage vs frequency

(b) Output power vs frequency

Figure 5.3: Stepper motor output values.

The frequency of the rotations for the fourth test was also plotted as a function of time (see figure 5.4). Since the wheel was assumed to be homogeneous in mass, the applied torque from the gravity and any potential vibrations would not affect the rotation of the wheel. This meant that the system equation (see equation 2.12) could be rewritten as

$$\ddot{\phi} = -\gamma\dot{\phi} \tag{5.1}$$

Which was possible to solve analytically with the solution:

$$\phi(t) = \phi(0)\mathrm{e}^{-\gamma t} \tag{5.2}$$

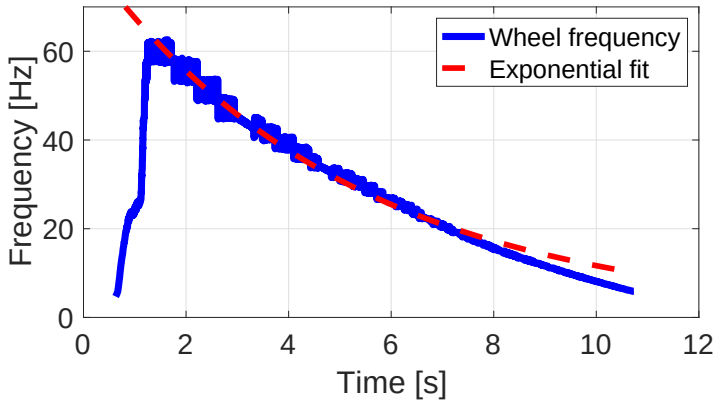

Figure 5.4: Estimated frequency and least square regression for one estimation of viscous damping constant.

Since the wheel was accelerated and then allowed to spin freely until it stopped, the constant γ could be estimated by fitting an exponential curve to the decelerating part of the frequency estimation. Due to the fact that the damping constant is dependent on the interia of the system (see equation 2.2), the damping constant was multiplied with the inertia of the wheel and then divided with the inertia of the pendulum of the

nominal system to be able to compare with the other tests and simulations. These calculations were performed for the four different tests. During these tests the wheel reached different maximum angular velocities. The results can be seen in Table 5.1. There it can also be seen that the tests with higher maximum angular velocity also have a lower estimated damping constant.

Table 5.1: Estimated values for viscous damping constant γ for three different tests.

Test #	γ [s^{-1}]	Maximum ω [Hz]
1	0.53	19
2	0.53	15
3	0.46	22
4	0.28	63
mean	0.45	

5.2 Test with vibrations generated by shaking table at ReVibe Energy

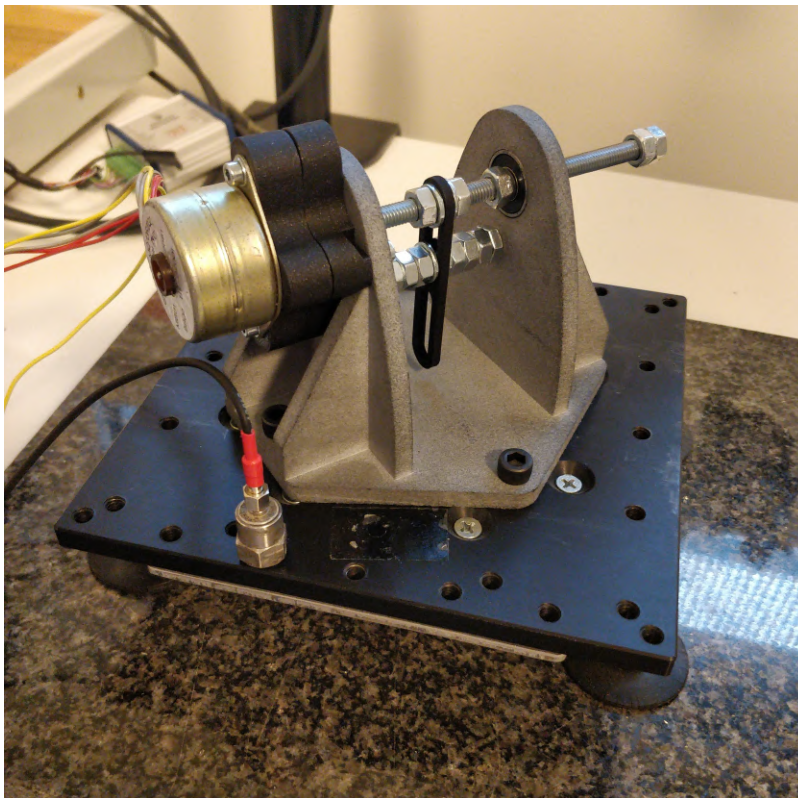

Figure 5.5: Test rig at ReVibe Energy with prototype attached on the shaking table.

The second test was conducted at ReVibe Energy's facilities, with the purpose to confirm the functionality of the prototype and test rig. A *Controlled Vibration, Electrodynamic Shaker (Model ED-5)* [29] was used to generate vertical vibrations, which were

measured with an accelerometer connected and stored to a computer (see Figure 5.5). The voltage was read accordingly with Figure 5.1 and recorded. The vibrational frequency was set to 14 Hz and the acceleration was slowly increased to 0.6 g, which was the lowest frequency and highest acceleration that was allowed for the shaker table, without risking any damage on the equipment. An initial angular rate of approximately 17 Hz was for multiple attempts, applied by hand to the system, to attempt to initiate rotations. The frequency, illustrated in Figure 5.6 was calculated based on the voltage data, generated by the stepper motor. The voltage was only stored from one of these attempts so the initial angular velocity applied probably varied among the attempts.

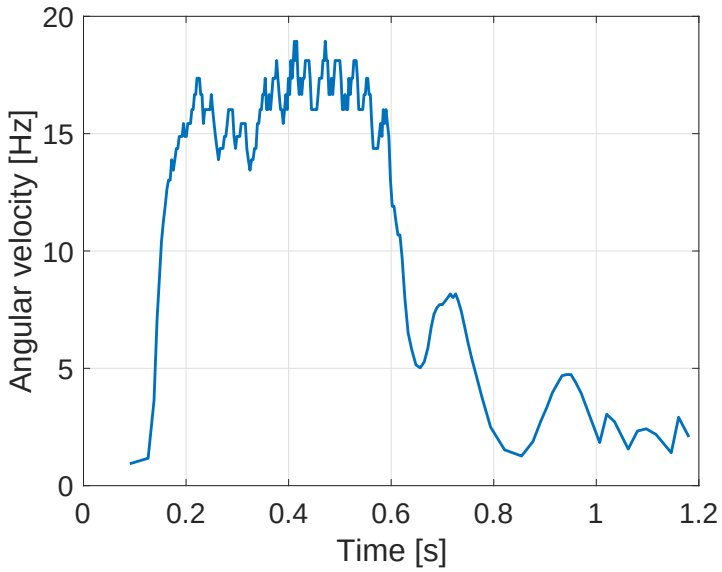

Figure 5.6: Pendulum frequency during test at ReVibe Energy

The pendulum length was initially set to the maximal value for the prototype of 50 mm. This length was decreased between the attempts until the minimum length of 13 mm was reached, but no continuous rotations were observed. When no attempts with the stepper motor attached succeeded, the stepper motor was removed to reduce the damping of the system, and increase the possibilities for continuous rotations. Despite the absence of the damping from the stepper motor, no rotations were observed.

As Figure 5.7a illustrates, there is a low probability to achieve rotating solutions with pendulum length 50 mm and initial angular velocity of 17 Hz. With the 13 mm pendulum length, however, there is a higher probability to achieve continuous rotations with this initial angular velocity (see Figure 5.7b).

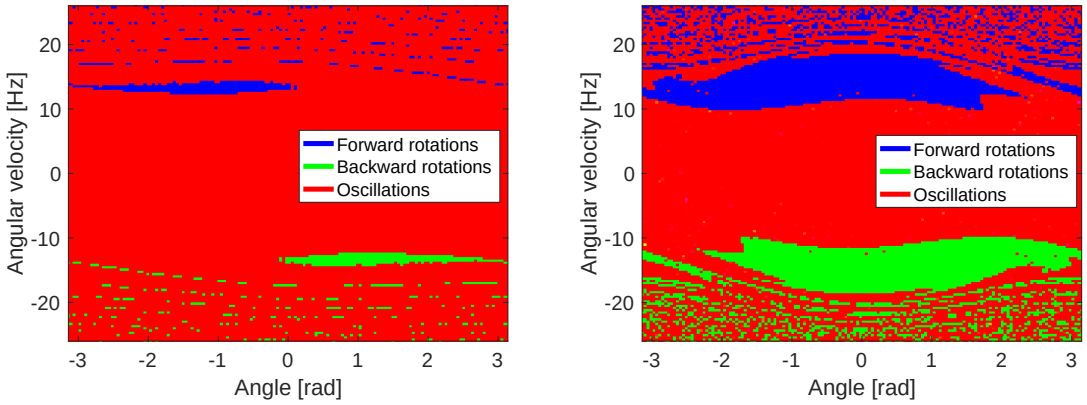

(a) Pendulum length of 50 mm

(b) Pendulum length of 13 mm

Figure 5.7: Results from simulating basin of attraction for system with parameters corresponding to the physical test with the shaking table.

5.3 Test with vibrations created by shaking the prototype on knee

To produce and measure vibrations that would lead to rotations of the pendulum, a smartphone was taped to the bottom of the prototype and the harvester was held in place on a knee in order to constrain the vibrations to only one dimension. The rig was then shaken using a bouncing foot movement. To initialise continuous rotations the frequency of the vibration was lowered and then accelerated up to approximately 6.5 Hz and lower amplitude.

An initialisation of continuous rotations can be seen in Figure 5.8b at about 12 seconds into the test. The continuous rotations were maintained between the time 13 and 34 seconds, illustrated in Figures 5.8c and 5.8d. When continuous rotations were achieved, the vibration amplitude and frequency was approximately 1.5 g and 6.5 Hz. The mean peak voltage during the continuous rotations was 1.3 V.

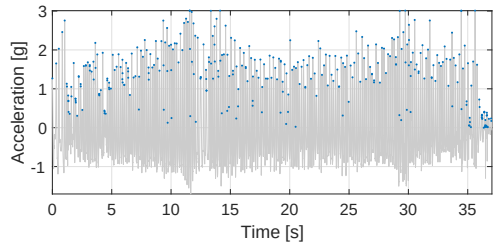

(a) Accelerometer data

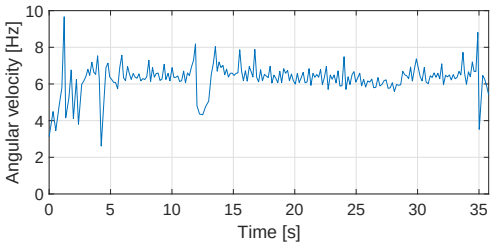

(b) Angular velocity of vibrations

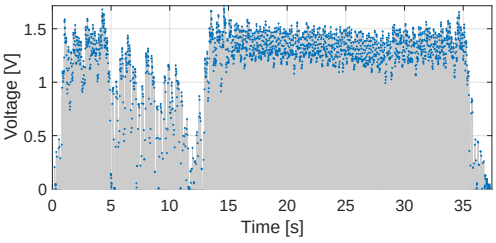

(c) Prototype voltage output

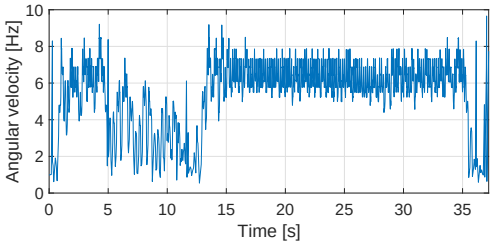

(d) Calculated pendulum angular velocity

Figure 5.8: Test data

The system was finally simulated with the measured values from the knee vibrations and the results can be seen in Figure 5.9. The simulation shows that if the pendulum manages to leave the basin of attraction corresponding to the low mean angular velocity, there is a higher probability to achieve full rotations.

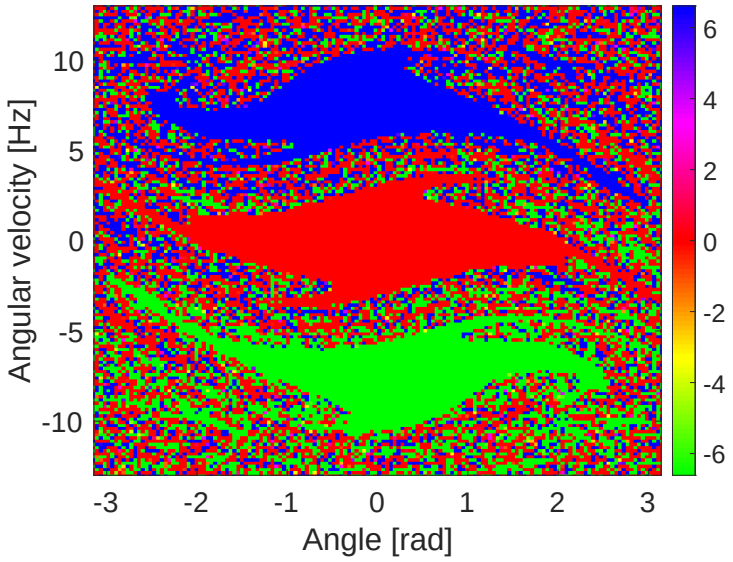

Figure 5.9: Color coded mean angular velocity simulation with measured vibration.

6

Discussion and future work

The study by Spreemann et al. [23] describes that performance in chaotic behaviour depends heavily on initial conditions, but the results from this thesis, however, demonstrates that the initial conditions almost have no affect on a chaotic system at all (see Figure 3.9b). A non-chaotic system, however, as the nominal system for example, depends heavily on the initial conditions illustrated in Figure 3.3a.

The simulations also show that the chaotic trajectories can be as good at translating the energy from the vibrations into rotations as the non-chaotic ones. This can be seen in the low dependence on initial condition and the high mean absolute velocity. One thing to consider however is that the chaotic systems are the ones where the vibrations have a large displacement in relation to the length of the pendulum. This could make it difficult to use this type of system if the environment is vibrating with a lower displacement.

It can be seen that the exponential curve fit in Figure 5.4 does not fit the recorded data completely. For example the frequency of the wheel decays faster than the curve fit for low frequencies, meaning that the damping constant extracted from the curve fit is lower than reality in this region. One interpretation of this is that the damping in the system does not result in an exponential decay of the angular velocity in this manner. This is also supported by the trend that the estimated constant becomes lower as the maximum angular velocity increases. However, the values extracted from the curve fit are somewhat lower than the value used in the simulations ($\gamma = 2$ $[s^{-1}]$ in the simulations and has a mean estimated value of 0.45 $[s^{-1}]$) meaning that the values chosen for the damping can compensate for this error to some extent.

During the test with the shaking table at ReVibe Energy, the system did not rotate despite the simulations showing that it is possible. There are some possible reasons for why this is. One is that the damping estimated from the test with the spinning wheel might not be correct. Another problem that was experienced during the test at ReVibe Energy was that the shaking table did not produce vibrations in one direction. Due to the motions of the pendulum, the table shook from side to side. The effect that these side forces have on the pendulum is another uncertainty in the test.

One complicating detail for this kind of system is that the damping constant is reversely proportional to the inertia of the pendulum as seen in equation 2.17. According to this equation a system with a certain damping constant and a higher inertia in the

pendulum will be able to handle a higher breaking torque from the generator than a system with a shorter or lighter pendulum with the same damping constant. A lower damping torque means that the induced current from the generator will have to be lower according to equation 2.15 which will lead to a lower power output.

When analysing the bandwidth of the system from the simulations, the basins of attractions for the rotating attractors shown in Figure 3.10 are small compared to the basins of attraction for the oscillating trajectories. This means that the initial conditions required to achieve full rotations are more difficult to find. Since the basin of attraction become smaller and smaller the closer to the boundaries the vibrations move, the rotations will become more and more difficult to find. Depending on how a system designed to operate in this region will be initialised the practical bandwidth of the system could be considered more narrow.

The resonant harvester has a single operating frequency with a certain bandwidth depending on the parameters of the harvester and the amplitude of the vibrations. The rotating harvester on the other hand has the advantage of being able to produce electricity at any tested frequency given that the amplitude of the system is strong enough to drive the pendulum into rotations or chaotic motion.

The rotational harvester also seem to have an advantage in its ability to handle changes in vibration. The results from changing the vibration frequency during simulation shows that a rotational harvester can to some extent handle changes in the vibrations while rotating. The tests have however only tested discrete changes in vibration frequency so more testing is needed before implementing a rotational energy harvesting system in an environment with changing vibrations.

The inductance in the stepper motor has not been used in the power calculations. This has the implications that the power output most likely is lower than what has been calculated since an inductance introduces a phase difference between current and voltage that has not been accounted for. This together with the choice of using a simple stepper motor as a generator instead of the DC-motor used in the model, makes the power calculations usable if viewed as a proof-of-concept. For more thorough estimations on maximum possible power output from the electrical and generator subsystems more work is needed.

7

Conclusions

This thesis has presented modelling, analysis, prototype development and verification of a rotational vibration energy harvester. As the simulations and the verification describes, it appear feasible to harvest vibrational energy with an eccentric mass.

The simulations show that this type of harvester is especially suited to operate in environments with large enough vibrations displacement that the system can rotate with chaotic trajectories. This is because this mode does not require any initial torque to be applied in order to reach the basin of attraction of the non-chaotic rotating trajectories. If the non-chaotic mode is to be used, further work needs to be done to identify how such a start up procedure would be designed to minimise the energy needed to reach continuous full rotations.

The rotational harvester is better suited for larger vibrations and lower frequencies compared to the linear harvesters that excel in higher vibration frequencies. The rotational harvester also has an advantage due to its ability to utilise vibrations from more than one direction. With further research and development the rotational harvesters can complement the linear to increase the application areas for vibration energy harvesters further.

Bibliography

[1] F. K. Shaikhab and S. Zeadallyc, "Energy harvesting in wireless sensor networks: A comprehensive review," *Renewable and Sustainable Energy Reviews*, vol. 55, pp. 1041–1054, 2016, [Online]. Available: https://doi.org/10.1016/j.rser.2015.11.010, Accessed on: 2021-05-31.

[2] J. Aponte-Luis, J. A. Gómez-Galán, F. Gómez-Bravo, M. Sánchez-Raya, J. Alcina-Espigado, and P. M. Teixido-Rovira, "An efficient wireless sensor network for industrial monitoring and control," *Sensors*, vol. 18, no. 182, 2018, [Online]. Available: https://doi.org/10.3390/s18010182, Accessed on: 2021-05-31.

[3] D. Spreemann and Y. Manoli, *Electromagnetic Vibration Energy Harvestin Devices*. Dordrecht: Springer, 2012, [Online]. Available: https://doi.org/10.1007/978-94-007-2944-5, Accessed on: 2021-05-31.

[4] H. Akinaga, "Recent advances and future prospects in energy harvesting technologies," *Japanese Journal of Applied Physics*, vol. 59, no. 11, 2020, [Online]. Available: https://doi.org/10.35848/1347-4065/abbfa0, Accessed on: 2021-05-31.

[5] X. Bai, Y. Wen, P. Li, and J. Yang, "Multi-resonant vibration energy harvester using a spiral cantilever beam," *IEEE International Ultrasonics Symposium*, pp. 1–4, 2012, [Online]. Available: https://doi.org/10.1109/ULTSYM.2012.0602, Accessed on: 2021-05-31.

[6] F. U. Khan and I. Ahmad, "Review of energy harvesters utilizing bridge vibrations," *Shock and Vibration*, vol. 2016, 2016, [Online]. Available: https://doi.org/10.1155/2016/1340402, Accessed on: 2021-05-31.

[7] C. Mathuna, T. O'Donnell, R. V. Martinez-Catala, J. Rohan, and B. O'Flynn, "Energy scavenging for long-term deployable wireless sensor networks," *Talanta*, vol. 75, no. 3, pp. 613–623, 2008, [Online]. Available: https://doi.org/10.1016/j.talanta.2007.12.021, Accessed on: 2021-05-31.

[8] C. B. Williams and R. B. Yates, "Analysis of a micro-electric generator for microsystems," *Sensors and Actuators A: Physical*, vol. 52, no. 1-3, pp. 8–11, 1996, [Online]. Available: https://doi.org/10.1016/0924-4247(96)80118-X, Accessed on: 2021-05-31.

[9] S. P. Beeby, M. J. Tudor, and N. M. White, "Energy harvesting vibration sources for microsystems applications," *Measurement Science and Technology*, vol. 17, no. 12, p. 175–195, 2006, [Online]. Available: https://iopscience.iop.org/article/10.1088/0957-0233/17/12/R01/meta, Accessed on: 2021-05-31.

[10] ReVibe Energy, "Product overview," 2021, [Online]. Available: https://revibeenergy.com/product-overview-harvesting/, Accessed on: 2021-04-14.

[11] *Powering the Internet of Things*, Gothenburg, Sweden: ReVibe Energy, 2021.

[12] J. Paradiso and T. Starner, "Energy scavenging for mobile and wireless electronics," *Pervasive Computing, IEEE*, vol. 4, pp. 18 – 27, 02 2005, [Online]. Available: https://doi.org/10.1109/MPRV.2005.9, Accessed on: 2021-05-31.

[13] T. von Büren, "Body-worn inertial electromagnetic micro-generators," Ph.D. dissertation, Information technology and Electrical Engineering, Eidgenössische Technische Hochschule Zürich, Zürich, Switzerland, 2006. [Online]. Available: https://doi.org/10.3929/ethz-a-005173297

[14] P. D. Mitcheson, T. C. Green, E. M. Yeatman, and A. S. Holmes, "Architectures for vibration-driven micropower generators," *Journal of Microelectromechanical Systems*, vol. 13, no. 3, pp. 429 – 440, 2004, [Online]. Available: https://doi.org/10.1109/JMEMS.2004.830151, Accessed on: 2021-05-31.

[15] Y. Bai, P. Tofel, Z. Hadas, J. Smilek, P. Losak, P. Skarvada, and R. Macku, "Investigation of a cantilever structured piezoelectric energy harvester used for wearable devices with random vibration input," *Mechanical Systems and Signal Processing*, vol. 106, pp. 303–318, 2018, [Online]. Available: https://doi.org/10.1016/j.ymssp.2018.01.006, Accessed on: 2021-05-31.

[16] R. Van Dooren, "Chaos in a pendulum with forced horizontal support motion: a tutorial," *Chaos, Solitons & Fractals*, vol. 7, no. 1, pp. 77–90, 1996, [Online]. Available: https://www.sciencedirect.com/science/article/pii/0960077995000186, Accessed on: 2021-05-31.

[17] M. Clifford and S. Bishop, "Rotating periodic orbits of the parametrically excited pendulum," *Physics Letters A*, vol. 201, no. 2, pp. 191–196, 1995, [Online]. Available: https://www.sciencedirect.com/science/article/pii/0375960195002552, Accessed on: 2021-05-31.

[18] S. Lenci, E. Pavlovskaia, G. Rega, and M. Wiercigroch, "Rotating solutions and stability of parametric pendulum by perturbation method," *Journal of Sound and Vibration*, vol. 310, no. 1, pp. 243–259, 2008, [Online]. Available: https://www.sciencedirect.com/science/article/pii/S0022460X0700630X, Accessed on: 2021-06-16.

[19] B. Koch and R. Leven, "Subharmonic and homoclinic bifurcations in a parametrically forced pendulum," *Physica D: Nonlinear Phenomena*, vol. 16, no. 1, pp. 1–

13, 1985, [Online]. Available: https://www.sciencedirect.com/science/article/pii/016727898590082X, Accessed on: 2021-05-31.

[20] W. CHESTER, "The Forced Oscillations of a Simple Pendulum," *IMA Journal of Applied Mathematics*, vol. 15, no. 3, pp. 289–306, 06 1975, [Online]. Available: https://doi.org/10.1093/imamat/15.3.289, Accessed on: 2021-05-31.

[21] M. Gitterman, *Chaotic Pendulum, The*. 5 Toh Tuck Link, Singapore 596224: World Scientific Publishing Company, 2010, [Online]. Available: https://ebookcentral.proquest.com/lib/chalmers/detail.action?docID=731266, Accessed on: 2021-05-31.

[22] E. I. Butikov, "Kapitza pendulum: A physically transparent simple explanation," 2017, [Online]. Available: http://butikov.faculty.ifmo.ru/InvPendulumPTSE.pdf, Accessed on: 2021-06-03.

[23] D. Spreemann, Y. Manoli, B. Folkmer, and D. Mintenbeck, "Non-resonant vibration conversion," *J. Micromech. Microeng.*, vol. 16, pp. 169 – 173, 2006, [Online]. Available: http://dx.doi.org/10.1088/0960-1317/16/9/S01, Accessed on: 2021-05-31.

[24] D. P. Arnold, "Review of microscale magnetic power generation," *IEEE TRANSACTIONS ON MAGNETICS*, vol. 43, pp. 3940 – 3951, 2007, [Online]. Available: https://doi.org/10.1109/TMAG.2007.906150, Accessed on: 2021-05-31.

[25] F. U. Khan, "Review of non-resonant vibration based energy harvesters for wireless sensor nodes," *J. Renewable Sustainable Energy*, vol. 8, no. 044702, 2016, [Online]. Available: https://doi.org/10.1063/1.4961370, Accessed on: 2021-05-31.

[26] A. Vikerfors, private communication, Jan. 2021.

[27] *ST32 UNI Stepper motor*, Dordrecht, The Netherlands: Premotec, 2000. [Online]. Available: https://premotec.home.xs4all.nl/pdf/stepper/ST32%20UNI.pdf, Accessed on: 2021-05-31.

[28] R. Teja, "What is Maximum Power Transfer Theorem (MPTT)?," Electronics Hubs. [Online]. Apr. 5, 2021. Available: https://www.electronicshub.org/maximum-power-transfer-theorem/ (accessed on: 2021-06-03).

[29] C. V. by CROWSON TECHNOLOGY, "5 lb load shaker," n.d., [Online]. Available: https://controlledvibration.com/product-item/5lb-load-shaker/#tab-id-2, Accessed on: 2021-06-03.